A Shapiro delay detection in the pulsar binary system PSR J1811–2405

C. Ng, L. Guillemot, P.C.C. Freire, M. Kramer, D.J. Champion, I. Cognard, G. Theureau, E.D. Barr

Monthly Notices
of the
ROYAL ASTRONOMICAL SOCIETY

MNRAS **493,** 1261–1267 (2020)
Advance Access publication 2020 February 6

doi:10.1093/mnras/staa337

A Shapiro delay detection in the pulsar binary system PSR J1811–2405

C. Ng [1,2★] L. Guillemot,[3,4] P. C. C. Freire [2★] M. Kramer,[2,5] D. J. Champion [2] I. Cognard,[3,4] G. Theureau[3,4,6] and E. D. Barr[2,7]

[1]*Dunlap Institute for Astronomy and Astrophysics, University of Toronto, 50 St George Street, Toronto, ON M5S 3H4, Canada*
[2]*Max-Planck-Institut für Radioastronomie, Auf dem Hügel 69, D-53121 Bonn, Germany*
[3]*Laboratoire de Physique et Chimie de l'Environnement et de l'Espace, LPC2E, CNRS-Université d'Orléans, F-45071 Orléans, France*
[4]*Station de Radioastronomie de Nançay, Observatoire de Paris, CNRS/INSU, F-18330 Nançay, France*
[5]*Jodrell Bank Centre for Astrophysics, University of Manchester, Alan Turing Building, Oxford Road, Manchester M13 9PL, UK*
[6]*LUTH, Observatoire de Paris, PSL Research University, CNRS, Université Paris Diderot, Sorbonne Paris Cité, F-92195 Meudon, France*
[7]*Centre for Astrophysics and Supercomputing, Swinburne University of Technology, Mail H30, PO Box 218, VIC 3122, Australia*

Accepted 2020 January 31. Received 2020 January 29; in original form 2019 November 1

ABSTRACT

This paper presents the first detection of Shapiro delay from the binary millisecond pulsar PSR J1811–2405. We report a 11σ measurement of the orthometric amplitude, $h_3 = 6.8(6) \times 10^{-7}$, and a 16σ measurement of the orthometric ratio, $\varsigma = 0.81(5)$. Given the relatively high orbital inclination, $i = 79(2)^\circ$, of this binary system, we obtain constraints on the companion mass of $m_c = 0.31^{+0.08}_{-0.06}\,M_\odot$. The pulsar mass is currently less well constrained, with a value of $2.0^{+0.8}_{-0.5}\,M_\odot$. The companion mass and the orbital period are in agreement with the prediction made by previous numerical calculations of the evolution of compact binary systems. From a study of the polarization, we find that the orbital inclination angle is $\sim 100^\circ$ and that PSR J1811–2405 is an orthogonal rotator. In addition, the μs-level timing precision together with its narrow profile makes PSR J1811–2405 a good candidate for inclusion in the pulsar timing arrays being used to detect nHz gravitational waves.

Key words: stars: neutron – pulsars: binaries – pulsars: individual: PSR J1811–2405.

1 INTRODUCTION

PSR J1811–2405 was discovered by the High Timing Resolution Universe Pulsar survey (Keith et al. 2010) conducted with the 64-m Parkes radio telescope. This millisecond pulsar binary system was initially published by Bates et al. (2011). PSR J1811–2405 was reported to be a typical low-mass binary pulsar likely with a Helium white dwarf (He-WD) companion in an orbit of roughly 6.27 d. No post-Keplerian (PK) parameters were detected at the time of the previous publication.

Using the best available radio timing ephemeris, Ng et al. (2014) detected gamma-ray pulsations from this pulsar in data from the *Fermi Gamma-ray Space Telescope* (*Fermi*; Atwood et al. 2009). In order to keep the radio ephemeris up to date and allow for accurate folding of all the gamma-ray data, this pulsar is observed regularly with the Nançay Radio Telescope (NRT). Thanks to this as well as a dedicated timing campaign with the Effelsberg Radio Telescope, we have timing data spanning a total of 6.9 yr. As a result of this timing project, we have detected the Shapiro delay for this system, and showed that it has a fairly edge-on orbital inclination.

First proposed by Shapiro (1964), the Shapiro delay is the retardation in the arrival times of a pulsar's pulses as they propagate through the curved space–time in the close vicinity of the binary companion. This effect is most readily observed in binary systems viewed nearly edge-on, and in some cases allows for precise measurements of the pulsar and companion masses, e.g. PSR J1614–2230 (Demorest et al. 2010). This and PSRs J0348+0432 and J0740+6620, with implied masses of 1.908 ± 0.016, 2.01 ± 0.04, and $2.14 \pm 0.10\,M_\odot$, respectively (Antoniadis et al. 2013; Arzoumanian et al. 2018; Cromartie et al. 2020), have effectively ruled out a number of equations of state (EOSs) for matter at densities above those of the atomic nucleus, including almost all currently proposed hyperon or boson condensate EOSs. This represents a very important constraint on the unknown state of matter at those densities (Özel & Freire 2016). None the less, precise neutron star mass measurements in general are hard to achieve because suitable systems are rare: Thus far, only 43 such measurements have been made.[1]

It is thus of great interest to obtain more neutron star mass measurements, in order to probe a wider parameter space of the

★ E-mail: cherrywyng@gmail.com (CN); pfreire@mpifr-bonn.mpg.de (PCCF)

[1]http://www3.mpifr-bonn.mpg.de/staff/pfreire/NS_masses.html

Table 1. Specifications of the observing systems employed for the timing observations in this work. f_c represents the associated receiver central frequency and B is the backend usable bandwidth, both in MHz. The number of TOAs generated from each data set is listed in the last column.

Backend	Receiver f_c (MHz)	B (MHz)	No. TOAs
Effelsberg PSRIX	1347	200	90
Nançay NUPPI	1484	512	2368
Nançay NUPPI	∼2200	512	74

EOS and to better understand the true distribution of neutron star masses.

This paper is organized as follows: In Section 2, we describe the radio timing observations conducted for PSR J1811–2405, including the instrumental set-up and the derivation of times of arrival. In Section 3, we present our updated timing solution and discuss results from the polarization study as well as from the Bayesian χ^2 analysis of the masses of the pulsar and its companion. We summarize our work in Section 4.

2 RADIO TIMING OBSERVATIONS

2.1 Observational set-up

Observations at the NRT began in 2012 as part of their regular gamma-ray pulsar follow-up timing campaign. The Nançay Ultimate Pulsar Processing Instrument (NUPPI; Desvignes et al. 2011) was employed to take coherently dedispersed timing data. The NUPPI data set has a high timing precision and is the longest span data set we have.

Despite its high instrumental sensitivity, the meridian nature of the NRT meant that PSR J1811–2405 could not be tracked for more than an hour. Hence, we conducted an intense timing campaign with daily observations during the 6.27 d orbit with the Effelsberg 100-m Radio Telescope in 2015 November. This campaign was designed to track the pulsar as long as possible on November 19 during superior conjunction. Shorter tracks were taken on either side of the superior conjunction observation to ensure good orbital coverage and to increase the confidence level of the Shapiro delay measurement. The Effelsberg observations were taken at the 1.4-GHz band using the central feed of the 7-beam receiver (P217mm). We used the PSRIX backend (Lazarus et al. 2016) that is based on the ROACH board and collects data in coherent dedispersion folding mode. One 1.6-h scan was carried out at a wavelength of 6 cm using the S60mm receiver although no pulsar signal was detected, setting an upper limit of flux density at $S_{4.9\,\mathrm{GHz}} < 0.02$ mJy. Refer to Table 1 for the specifications of all the receivers employed in this timing analysis.

2.2 Derivation of times of arrival and timing solution

The PSRCHIVE data analysis package (Hotan, van Straten & Manchester 2004) was used for the radio timing data reduction. Each observation was corrected for dispersion and folded at the predicted topocentric pulse period. We co-added high signal-to-noise observations and created noise-free reference template for each observing frequency using wavelet smoothing as implemented in the PSRCHIVE program of PSRSMOOTH (Demorest et al. 2015). We convolved the template with each individual profile to produce a time of arrival (TOA) (Taylor 1992). Multiple TOAs per observation were generated when possible, by downsampling the bandwidth to four frequencies and summing over every 10 min. This is appropriate for the accurate measurement of orbital effects such as Shapiro delay for a 6-d binary like PSR J1811–2405. The DE421 Solar system ephemeris of the Jet Propulsion Laboratory (Folkner, Williams & Boggs 2009) was used to transform the TOAs to the Solar system barycentre. Finally, the TEMPO2 software package (Hobbs, Edwards & Manchester 2006) was used to fit a timing model to all TOAs, taking into account the astrometry, spin, and orbital motion of the pulsar.

As mentioned in Ng et al. (2014), PSR J1811–2405 lies very close to the ecliptic plane with ecliptic coordinates $(\lambda, \beta) = (272^\circ.586, -0^\circ.675)$. With λ so close to 270°, the uncertainty in β will only pertain to the declination when transforming in equatorial coordinates. We hence fixed proper motion in declination at zero for the rest of the analysis. The parallax was also fixed at zero as the timing precision of our data is not high enough for measuring parallax with significance.

A careful modelling of the dispersion measure (DM) is very important for this work because any unaccounted temporal DM variations can degrade the precision of a Shapiro delay measurement. The fact that PSR J1811–2405 is on the ecliptic plane also means that it is more susceptible to solar wind DM contribution. We used the solar wind model implemented by default in TEMPO2 (where the density of electrons is proportional to $1/r_\odot^2$, with $r_\odot$ being the distance to the Sun; see Edwards, Hobbs & Manchester 2006). However, instead of the default value of 4 electrons cm^{-3} at the Earth's distance from the Sun proposed by Edwards et al. (2006), we used 5 electrons cm^{-3}, which was found to yield slightly better results by Arzoumanian et al. (2018). The timing baseline of PSR J1811–2405 coincides in time with the NANOGrav timing baseline, thus warranting the use of the same electron model. We disregarded any observations that were taken with a solar elongation angle $<15^\circ$.

This simple model is not enough to describe DM variations from the Solar wind, and it certainly cannot describe DM variations caused by the ionized interstellar medium. In order to do that, we must in addition use the DMX parametrization in the TEMPO2 software package. This a piecewise linear fit of temporal DM variations (see NANOGrav Collaboration 2015, for a detailed definition). It can be used to measure DM variations with a bin size of several days. In the bottom panel of Fig. 1, we used a 11-d DMX window and showed that there is a temporal DM variation of the order of 0.005 cm^{-3} pc over the course of our timing data. Alternatively, we also attempted to model this DM variation using DM derivatives. However, small time-scale variations seen in Fig. 1 meant that even including up to the eighth DM derivative, the model still deviates visibly from the data. We hence concluded that DMX appears to be a more reasonable approximation of the DM trend compared to using DM derivatives. We note that neither DM model has predictive power outside the range of data we have here.

Since PSR J1811–2405 has a very circular orbit with an eccentricity of the order of 10^{-6}, we used the ELL1 and ELL1H orbital models (Lange et al. 2001; Freire & Wex 2010) to characterize it. In the more commonly used orbital models, like the BT (Blandford & Teukolsky 1976) and DD (Damour & Deruelle 1986) models, there is a large covariance between two orbital parameters, the longitude of periastron (ω), and the epoch of periastron (T_0); this becomes extremely large for small orbital eccentricities. The ELL1 and ELL1H models avoid this by replacing those parameters and the orbital eccentricity e by the Laplace–Lagrange parameters ($\epsilon_1 = e\sin\omega$ and $\epsilon_2 = e\cos\omega$) and the time of ascending node passage (T_{asc}); these have very small correlations among themselves. The ELL1 and

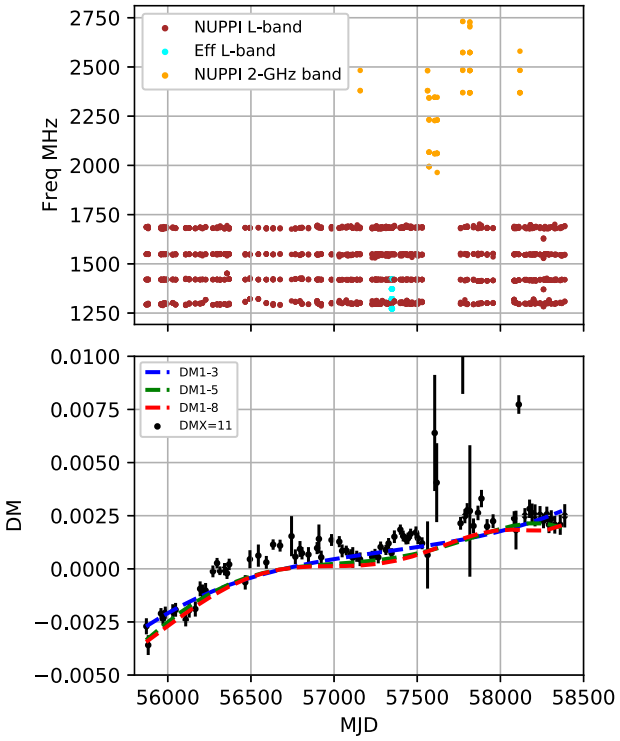

Figure 1. Top panel: the temporal coverage of observing frequency of the coherently dedispersed timing data used in this analysis. We create four subbands per observation when possible. The plot is colour coded to show the different telescopes and backends, including Nançay NUPPI at the *L* band (brown), Nançay NUPPI at 2 GHz (orange), and Effelsberg PSRIX (cyan). Bottom panel: DM variation as a function of time, measured by fitting for DMX with a window of 11 d (black) in TEMPO2. There are small time-scale DM variations that cannot be modelled properly using DM derivatives (blue: up to the third derivatives; green: up to the fifth derivative; red: up to the eighth derivative).

ELL1H models are approximate; they should only be used when the ignored term (with an amplitude of $x.e^2 = 7.0 \times 10^{-12}$ lt-s) is smaller than the timing precision ($T_{\rm rms}/\sqrt{N} = 3.6 \times 10^{-8}$ s); this is certainly the case for PSR J1811–2405. This implies that ignoring that term will have, in this case, no other consequences; in particular, it will have no effect on the measurement of the Shapiro delay.

Towards the end of the timing analysis when the reduced χ^2 is close to one, we can assume that the timing model provides a reliable fit to the data. As a last step, we compensated for any remaining systematics by calculating backend-specific weighing correction (also known as 'EFAC' in TEMPO2). These coefficients were applied to scale the TOA uncertainties such that the reduced χ^2 is unity for each individual data set. This procedure yields more conservative and realistic estimates of the uncertainties in the timing parameters.

The timing solution of PSR J1811–2405, obtained using the ELL1H model, can be found in Table 2. Only coherently dedispersed timing data from Nançay and Effelsberg were employed in the timing analysis because they have the highest precision and represent the most homogeneous data set.

The main new result from the timing is a clear detection of the Shapiro delay. Fig. 2 compares the timing residuals when Shapiro delay is and is not taken into account. The signature sharp peak of a Shapiro delay can be seen clearly around phase 0.25, where the Earth-pulsar line of sight passes nearest to the companion as defined by the ELL1 and ELL1H binary models.

Table 2. TEMPO2 best-fitting parameters for PSR J1811–2405. Values in parentheses are the nominal 1σ uncertainties in the last digits.

Spin and astrometric parameters	
Right ascension, α (J2000)	18:11:19.854050(19)
Declination, δ (J2000)	−24:05:18.422(10)
Proper motion in R.A., μ_α (mas yr^{-1})	0.53(6)
Spin period, P (ms)	2.660 593 276 877 44(2)
Period derivative, $\dot{P}$	$1.337\,56(3) \times 10^{-20}$
Dispersion measure, DM (cm^{-3} pc)	60.6196(2)
Rotation measure (rad m^{-2})	21(9)
Binary parameters	
Orbital model	ELL1H
Orbital period, $P_{\rm orb}$ (days)	6.272 301 969 15(11)
Projected semimajor axis, x (lt-s)	5.705 6569(8)
Epoch of ascending node, $T_{\rm asc}$ (MJD)	56327.90581153(2)
$e\sin\omega$, ϵ_1	$9.9(9)\times 10^{-7}$
$e\cos\omega$, ϵ_2	$5.0(3)\times 10^{-7}$
Orthometric amplitude, h_3 (μs)	0.68(6)
Orthometric ratio, ς	0.81(4)
Derived parameters	
Inferred eccentricity, e	$1.11(8)\times 10^{-6}$
Longitude of periastron, ω (°)	62(2)
Mass function, f ($M_\odot$)	0.005 069 27(2)
Companion mass, m_c ($M_\odot$)	0.26(6)
$\sin i$	0.978(12)
Orbital inclination from Bayesian analysis, i (°)	$76.2^{+2.8}_{-3.2}$
Companion mass from Bayesian analysis, m_c ($M_\odot$)	$0.31^{+0.08}_{-0.06}$
Pulsar mass from Bayesian analysis, m_p ($M_\odot$)	$2.0^{+0.8}_{-0.5}$
DM-derived distance (kpc)†	1.8
Intrinsic period derivative, $\dot{P}_{\rm int}$	$1.284(15) \times 10^{-20}$*
Characteristic age, τ_r (Gyr)	3.15
Characteristic dipole surface magnetic field	1.9
Strength at equator, $B_{\rm eq}$ (10^8 G)	–
Spin-down power, $\dot{E}$ (10^{34} erg s^{-1})	2.7
Timing model	
Binary model	ELL1
Solar system ephemeris	DE421
Timing epoch (MJD)	56330
First TOA (MJD)	55871.6
Last TOA (MJD)	58386.9
Weighted RMS residuals (μs)	1.81
Reduced χ^2	1.3

Notes. *We have fixed the unconstrained proper motion in declination (μ_δ) at zero because PSR J1811–2405 is very close to the ecliptic plane. The transverse velocity is therefore also not measurable. The derived $\dot{P}_{\rm int}$ represents an upper limit, obtained limit without correcting for any Shklovskii contribution (Shklovskii 1970) in μ_δ.
†Both the NE2001 (Cordes & Lazio 2002) and YMW2016 (Yao, Manchester & Wang 2017) electron density models yield the same distance estimate.

In the ELL1 model, the Shapiro delay is characterized by two PK parameters, the range (r) and shape (s) (Damour & Taylor 1992; Will 1993), where, assuming that general relativity (GR) is the correct description of gravity, $r = T_\odot m_c$ and $s = \sin i$ (here $T_\odot \equiv GM_\odot c^{-3} = 4.925\,490\,947\,641\,2675$ μs is the mass of the Sun in units of time). From these two parameters, we obtain $m_c = 0.26(6)\,M_\odot$ and $\sin i = 0.978(12)$. In the ELL1H model, the Shapiro delay is described by two different PK parameters, the orthometric ratio ς and amplitude h_3. Assuming GR, these are given

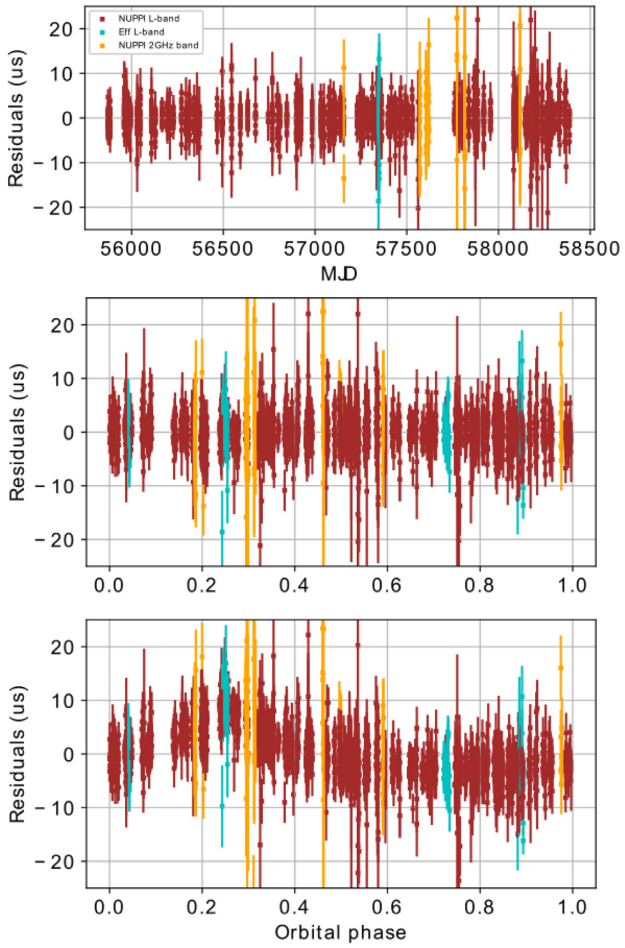

Figure 2. Timing residuals for PSR J1811–2405 as a function of MJD (top) and orbital phase (middle, bottom). TOAs are colour coded to show different telescopes and backends, including Nançay NUPPI at the *L* band (brown), Nançay NUPPI at 2 GHz (orange), and Effelsberg PSRIX (cyan). The middle panel shows the best-fitting residuals when all parameters including the Shapiro delay are fitted for. The bottom panel shows the residuals if sin *i* and m_c are set to zero and all other parameters are fixed at their best-fitting values. The expected characteristic signature can be seen at an orbital phase of 0.25. The error bars represent the 1σ uncertainties of the TOA measurements.

by $\varsigma = \frac{\sin i}{1+|\cos i|}$ and $h_3 = T_\odot m_c \varsigma^3$ (Freire & Wex 2010). These two parameters have much smaller correlation than *r* and *s*, and hence provide a better description of the m_c and *i* constraints derived from the Shapiro delay, particularly when the signal is weak. We report a highly significant (11σ) h_3 of $6.8(6)\times 10^{-7}$ and a 16σ measurement of $\varsigma = 0.81(5)$; these yield mass and inclination estimates similar to those derived in the ELL1 model. In Fig. 3, we can see that these two parameters provide a good description of the regions of the cos *i*–m_c plane where the system is most likely to be located. A detailed analysis of the mass and inclination constraints is presented in Section 3.2.

3 RESULTS AND DISCUSSION

3.1 Polarization study

The Effelsberg timing observations recorded the four Stokes parameters in each frequency channel and thus can be used to study the polarization profile. We polarization calibrated each observation for the differential gain and phase between the feeds with an observation of the noise diode coupled to the receptors in the feeds. We made sure that the polarization calibration is taken adjacent to the targeted pulsar observations. In additional to the Effelsberg data sets, PSR J1811–2405 was also followed up at the Parkes 64-m radio telescope initially after its discovery. Incoherently dedispersed Parkes Digital Filterbank systems (DFB) are available at the *L* band. A few observations have also been taken using the 10/50 cm receiver (Granet et al. 2005), which allow for the study of pulsar profile variations across frequencies. The Parkes observations were flux calibrated by using an averaged observation of Hydra A and the Effelsberg observation with the quasar 3C 353.

Fig. 4 shows the integrated polarization profiles of PSR J1811–2405 in total intensity, linear polarization, and circular polarization. We have arbitrarily aligned the main pulse at phase 0.4 across the three available observing frequencies. Our best 732 MHz profile comes from the co-adding of 4.1 h of Parkes APSR coherently dedispersed data. Our best *L*-band profile comes from the co-adding of 14.6 h of Parkes DFB incoherently dedispersed data. At 3100 MHz, a total of 4.7 h of incoherently dedispersed Parkes DFB observations are available. We attempted to measure the observed Faraday rotation by fitting the position angle (PA) variations at the *L* band across the 256 MHz band and obtained a rotation measure (RM) of 21(9) rad m^{-2}. The profiles shown in Fig. 4 have had their RM corrected.

PSR J1811–2405 has a profile comprising two main components: a main pulse and an interpulse. The interpulse appears roughly 0.45 in phase after the main pulse. We can also see that there is significant profile evolution across observing frequencies, as the strength of the interpulse decreases from being almost as bright as the main pulse at 3100 MHz to being almost unidentifiable at 735 MHz. The emission of the main pulse changes handedness in circular polarization, which is most obvious at 1369 MHz. The interpulse is strongly linearly polarized, especially at 3100 MHz. PSR J1811–2405 appears to have higher flux at lower observing frequencies, with a peak flux density of only a few mJy at 3100 MHz but over 60 mJy at 732 MHz. Such a steep spectral index is typical of pulsars.

We modelled the observed PA swing according to the Rotating Vector Model (RVM; Radhakrishnan & Cooke 1969). As detailed in Lorimer & Kramer (2004), the RVM can in principle provide insights on the magnetic inclination angle, α, as well as the viewing angle between the observer and the spin axis, ζ. We followed the procedure of a least-squares fit similar to that described in Berezina et al. (2017), by stepping through a range of α and ζ while simultaneously minimizing the reference phase Φ_0 and the reference PA Ψ_0 of the RVM at each grid point. This results in the 1σ χ^2 contour shown in Fig. 5. From the system parameters, we can expect PSR J1811–2405 to have undergone an extended recycling process, which not only transferred masses but also orbital angular momentum. As a result of this accretion phase, the spin angular momentum of the pulsar aligned with the orbital angular momentum over time. Hence, in order for the pulsar beam to be visible to a terrestrial observer, the viewing angle ζ must be roughly consistent with the orbital inclination angle (within the uncertainty of the angular radius of the pulsar beam, ρ, cf. Guillemot & Tauris 2014). We can thus expect $\zeta \approx i$. From the Shapiro delay measurements, we can only determine sin *i*; hence, both *i* and $180^\circ - i$ are possible. With this in mind, we mark the value of *i* and $180^\circ - i$ from our pulsar timing Shapiro delay on Fig. 5 as two horizontal bands, at

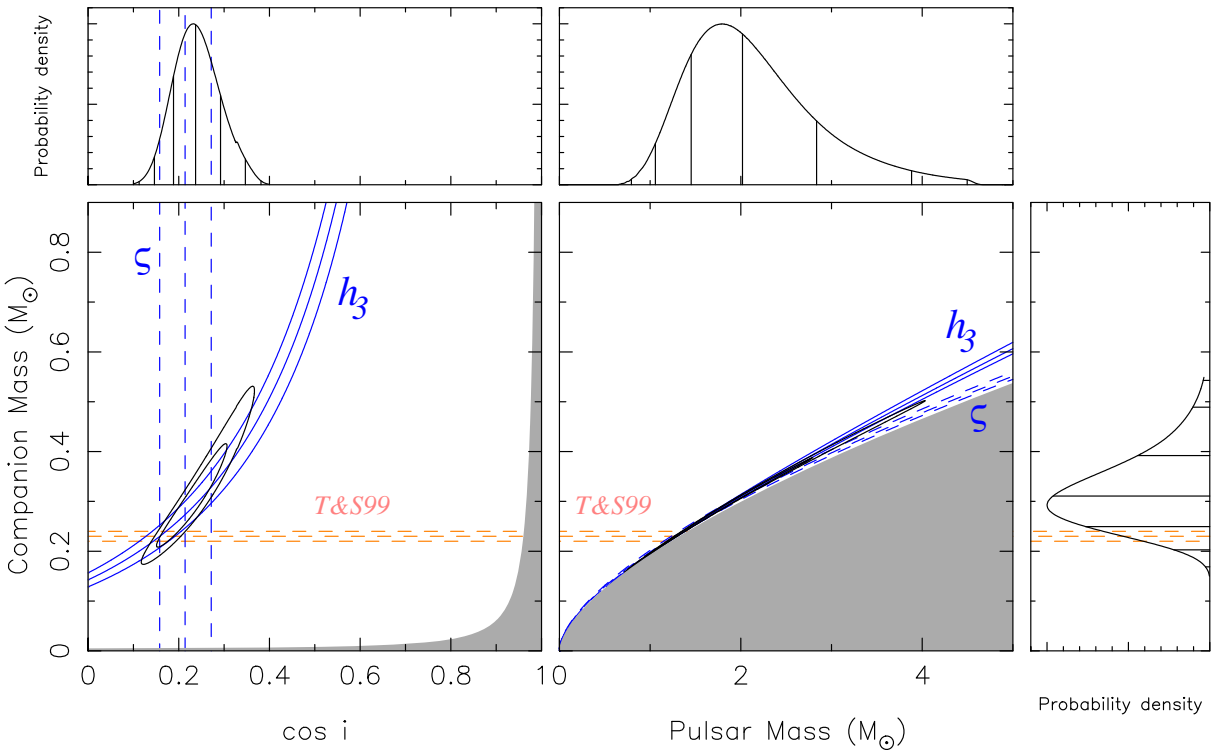

Figure 3. Shapiro delay constraints on the masses and orbital inclination of PSR J1811–2405. The black contours contain 68.27 and 95.45 per cent of the total probabilities of the 2D pdfs from the Bayesian χ^2 analysis. The blue lines correspond to the nominal and $\pm1\sigma$ uncertainties associated with the two orthometric parameters, ς (dashed line) and h_3 (solid line). The pink lines labelled as T&S99 represent the range of companion masses predicted by Tauris & Savonije (1999) for the orbital period of this system. Left: cos *i*–m_c plane. The grey area is excluded by $m_p > 0$. Right: m_p–m_c plane. The grey area is excluded by $\sin i \leq 1$. The lateral panels are projected 1D pdfs of cos *i*, m_p, and m_c, respectively.

79° and 101°, respectively. The width of these horizontal bands represents the uncertainty on *i*.

The intersection region of the polarimetry and orbital inclination favours a solution with $\alpha = 92°$ and $\zeta = 79.8°$, indicating that the true underlying orbital inclination angle is $i = 180° - 79.8° \sim 100°$. This α value also indicates that PSR J1811–2405 is an orthogonal rotator, which is consistent with the fact that we see an interpulse from the pulse profile. It is sometimes possible to obtain further constraints on α through a fitting of the pulse width, together with an assumption of a filled emission beam. However, the duty cycle of PSR J1811–2405 is relatively low and only the width of the main peak can be measured, which limits the reliability of this analysis. This is not unusual for MSPs, especially when low-level components are present as in the case of PSR J1811–2405.

Guillemot & Tauris (2014) analysed a sample of MSPs with ζ constraints, and found marginal evidence for different viewing angle distributions between gamma-ray-detected and undetected energy and nearby MSPs. They postulated that gamma-ray-undetected MSPs are seen under small viewing angles. PSR J1811–2405 is detected in gamma-rays and is seen under a large viewing angle, and thus seems to follow the trend. We also compared the gamma-ray profile of PSR J1811–2405 with the light-curve models presented in Romani & Watters (2010). Qualitatively, we found good agreement with their light curve corresponding to $(\alpha, \zeta) = (90°, 80°)$. We do not see obvious preference between the 'two pole caustic' and the outer gap model.

3.2 Pulsar mass constraint from the Shapiro delay measurements

As described by Splaver et al. (2002), we can estimate the masses and their uncertainties for the pulsar (m_p) and its companion by performing a Bayesian χ^2 analysis in the m_c–cos *i* plane. We stepped through a regular grid ranging from $0.15\,M_\odot \leq m_c < 0.55\,M_\odot$ and from $0.1 \leq \cos i < 0.4$, involving a total of 150×400 trial values. The assumption of a flat cos *i* plane can be justified if we consider the binary orbit to be randomly oriented in space. For each of these $m_c - \cos i$ pairs, we calculated the corresponding *r* and *s* to be held fixed. We fit for all other timing parameters and record the final χ^2. Fig. 3 shows the resultant χ^2 map, from which 2D probability distribution functions (pdfs) can be derived. The black contours represent the 68.27 and 95.45 per cent of the total probability, which is consistent with that from the fitting of h_3 and ς (blue lines) using the orthometric parametrization.

We can then marginalize the 2D pdfs by projecting them on to the m_c, cos *i*, and m_p axes. From these 1D pdfs, we obtain $m_p = 2.0^{+0.8}_{-0.5}\,M_\odot$, $m_c = 0.31^{+0.08}_{-0.06}\,M_\odot$, and $i = 76°.2^{+2°.8}_{-3°.2}$, where the quoted values are the medians together with the $\pm1-\sigma$ interval. The current value of m_p is not yet very well constrained but it could be improved with some more years of pulsar timing.

The detection of other PK parameters such as the orbital period variation ($\dot{P}_{orb}$) and the variation in the longitude of periastron ($\dot{\omega}$) could, in a more compact and eccentric system, have helped to narrow down the pulsar mass range and to conduct self-consistency tests of GR and other theories of gravity. For this system, a $\dot{P}_{orb}$

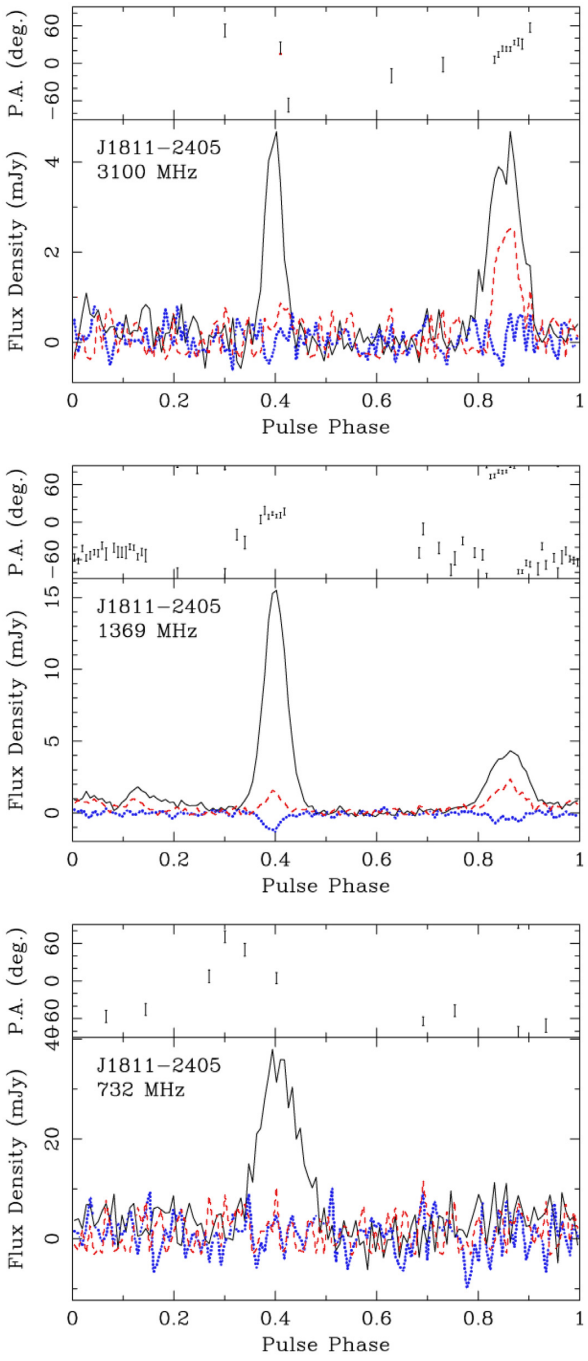

Figure 4. Polarization profiles of PSR J1811–2405 at (top) 3100 MHz from Parkes, (middle) 1369 MHz from Effelsberg, and (bottom) 732 MHz from Parkes. The upper panel of each figure shows the RM-corrected PA variation in longitude with respect to the celestial north. Only PAs with signal-to-noise ratios >3 are shown. The lower panel shows the integrated profile of total intensity (black solid line), linear polarization (red dashed line), and circular polarization (blue dotted line).

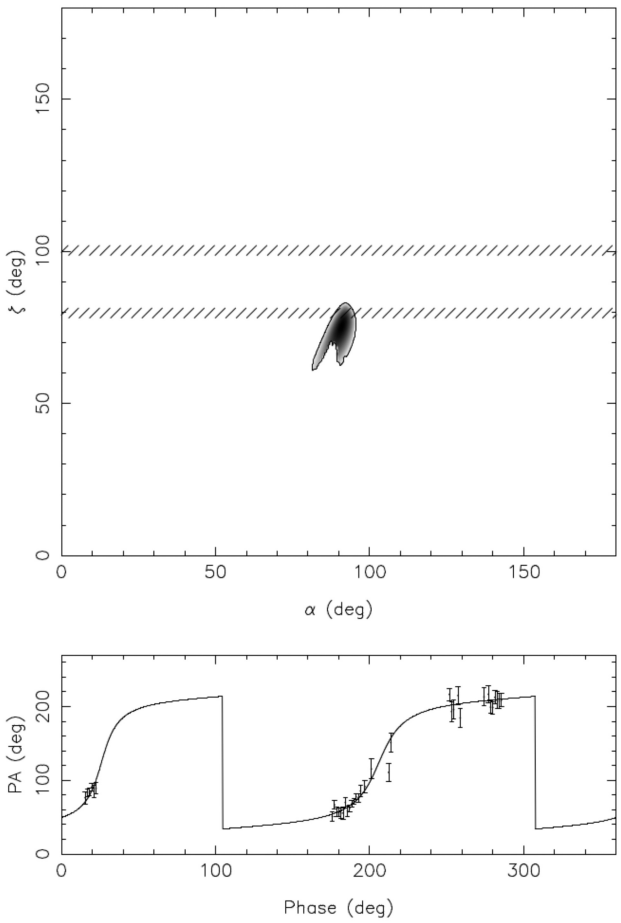

Figure 5. Main panel: System geometry for PSR J1811–2405 from a least-squares fit of the RVM to the PA. The contour indicates 1σ best-fitting region of α and ζ. The orbital constraints from our Shapiro delay measurement are marked as two horizontal bands. Bottom panel: The corresponding RVM fit for $\alpha = 92^\circ$ and $\zeta = 79.8^\circ$ is shown. An orthogonal shift is applied for the second group of points, as well as a 180° phase shift between the first and third groups.

value of the order of 10^{-16} is predicted from orbital decay due to GR, which is too small to be easily separated from kinematic effects due to the Galactic acceleration and the Shklovskii effect (Shklovskii 1970); hence, we do not expect to measure any intrinsic $\dot{P}_{\rm orb}$ in the near future. If we assume a pulsar mass of 1.5 $M_\odot$, for an orbital inclination of 79°, one can expect an $\dot{\omega}$ of 0.0136° yr^{-1}. Currently, we measure ω with a precision of 0.7°. This means that we will have to wait at least 50 yr to achieve a 1σ measurement of $\dot{\omega}$.

A more promising improvement can be achieved with the MeerKAT (Bailes et al. 2018) and even better, when the Square Kilometre Array (Stappers et al. 2018) comes online, which will most certainly provide much better constraints on the Shapiro delay measurement.

3.3 Evolution model

Tauris & Savonije (1999) conducted numerical calculations on the non-conservative evolution of close binary systems. They suggested that for diverging LMXBs with a donor mass $< 2\,M_\odot$ and a 1.3 $M_\odot$ accreting neutron star, if the orbital period is greater than the orbital bifurcation period, i.e. $P_{\rm orb} > P_{\rm bif}$ ($\simeq$2 d), then the system should follow a positive correlation between the orbital period and the mass of the final He-WD companion, quantified by equations (20) and (21) in Tauris & Savonije (1999).

PSR J1811–2405 belongs to this type of diverging system, with $P_{\rm orb} = 6.27$ d. In Fig. 3, we overplot the range of companion masses predicted by Tauris & Savonije (1999) for the orbital period of this system. The measurement of $m_{\rm c}$ is consistent with the prediction of

Tauris & Savonije (1999), but because of its large uncertainties, it cannot yet test the relation. We note that if the companion has the predicted mass, then the Shapiro delay parameters would imply a pulsar mass of around 1.3 $M_\odot$. It would also mean a cos i of ± 0.16, which equals to $i \sim 81^\circ$ or 99°. This is in agreement with the polarization estimate, and matches the orthogonal rotator scenario.

4 SUMMARY

We present an updated radio timing solution for the binary system PSR J1811–2405. An extended timing campaign and high-precision coherently dedispersed observations have allowed for the first detection of the relativistic Shapiro delay. We measured the orthometric amplitude h_3 and ratio ς with high significance. By conducting a Bayesian χ^2 analysis, we obtained constraints on the companion mass to be $m_c = 0.31^{+0.08}_{-0.06}\,M_\odot$ and a less well constrained pulsar mass of $m_p = 2.0^{+0.8}_{-0.5}\,M_\odot$.

The companion mass is in agreement with the theoretical m_c–P_{orb} correlation obtained by Tauris & Savonije (1999). From the polarization study, we obtained a solution of $\alpha = 92^\circ$ and $\zeta = 79.8^\circ$, indicating that the true underlying orbital inclination angle is $i \sim 100^\circ$, consistent with PSR J1811–2405 being an orthogonal rotator. The high timing precision and sharp profile of PSR J1811–2405 make it a good candidate to be included in a pulsar timing array to aid the gravitational-wave detection effort. With a longer timing baseline, we can then expect improvements in the precision of the pulsar mass measurement.

ACKNOWLEDGEMENTS

The Parkes Observatory is part of the Australia Telescope National Facility, which is funded by the Commonwealth of Australia for operation as a National Facility managed by CSIRO. This work was partly based on observations with the 100-m telescope of the MPIfR (Max-Planck-Institut für Radioastronomie) at Effelsberg. The Nançay Radio Observatory is operated by the Paris Observatory, associated with the French Centre National de la Recherche Scientifique (CNRS). We also thank Marina Berezina, Eleni Graikou, and Gregory Desvignes for advice on Effelsberg data calibration, as well as Andrew Cameron for carefully reading the manuscript.

REFERENCES

Antoniadis J. et al., 2013, Science, 340, 448
Arzoumanian Z. et al., 2018, ApJS, 235, 37
Atwood W. B. et al., 2009, ApJ, 697, 1071
Bailes M. et al., 2018, preprint (arXiv:1803.07424)
Bates S. D. et al., 2011, MNRAS, 416, 2455
Berezina M. et al., 2017, MNRAS, 470, 4421
Blandford R., Teukolsky S. A., 1976, ApJ, 205, 580
Cordes J. M., Lazio T. J. W., 2002, preprint (astro-ph/0207156)
Cromartie H. T. et al., 2020, Nat. Astron., 4, 72
Damour T., Deruelle N., 1986, Ann. Inst. Henri Poincaré Phys. Theór., 44, 263
Damour T., Taylor J. H., 1992, Phys. Rev. D, 45, 1840
Demorest P. B., Pennucci T., Ransom S. M., Roberts M. S. E., Hessels J. W. T., 2010, Nature, 467, 1081
Demorest P. et al., 2015, Am. Astron. Soc. Meeting Abstr., 225, 346.01
Desvignes G., Barott W. C., Cognard I., Lespagnol P., Theureau G., 2011, in Burgay M., D'Amico N., Esposito P., Pellizzoni A., Possenti A., eds, AIP Conf. Proc. Vol. 1357, A New Pulsar Instrumentation at the Allen Telescope Array and the Nancay Radio Telescope. Am. Inst. Phys., New York, p. 349
Edwards R. T., Hobbs G. B., Manchester R. N., 2006, MNRAS, 372, 1549
Folkner W. M., Williams J. G., Boggs D. H., 2009, Interplanet. Netw. Prog. Rep., 178, C1
Freire P. C. C., Wex N., 2010, MNRAS, 409, 199
Granet C. et al., 2005, IEEE Antennas Propag. Mag., 47, 13
Guillemot L., Tauris T. M., 2014, MNRAS, 439, 2033
Hobbs G. B., Edwards R. T., Manchester R. N., 2006, MNRAS, 369, 655
Hotan A. W., van Straten W., Manchester R. N., 2004, Publ. Astron. Soc. Aust., 21, 302
Keith M. J. et al., 2010, MNRAS, 409, 619
Lange C., Camilo F., Wex N., Kramer M., Backer D. C., Lyne A. G., Doroshenko O., 2001, MNRAS, 326, 274
Lazarus P., Karuppusamy R., Graikou E., Caballero R. N., Champion D. J., Lee K. J., Verbiest J. P. W., Kramer M., 2016, MNRAS, 458, 868
Lorimer D. R., Kramer M., 2004, Handbook of Pulsar Astronomy, Vol. 4, Cambridge Univ. Press, Cambridge
NANOGrav Collaboration, 2015, ApJ, 813, 65
Ng C. et al., 2014, MNRAS, 439, 1865
Özel F., Freire P., 2016, ARA&A, 54, 401
Radhakrishnan V., Cooke D. J., 1969, Astrophys. Lett., 3, 225
Romani R. W., Watters K. P., 2010, ApJ, 714, 810
Shapiro I. I., 1964, Phys. Rev. Lett., 13, 789
Shklovskii I. S., 1970, Sov. Astron., 13, 562
Splaver E. M., Nice D. J., Arzoumanian Z., Camilo F., Lyne A. G., Stairs I. H., 2002, ApJ, 581, 509
Stappers B. W., Keane E. F., Kramer M., Possenti A., Stairs I. H., 2018, Phil. Trans. R. Soc. London Ser. A, 376, 20170293
Tauris T. M., Savonije G. J., 1999, A&A, 350, 928
Taylor J. H., 1992, Phil. Trans. R. Soc.: Phys. Sci. Eng., 341, 117
Will C. M., 1993, Theory and Experiment in Gravitational Physics. Cambridge Univ. Press, Cambridge
Yao J. M., Manchester R. N., Wang N., 2017, ApJ, 835, 29

This paper has been typeset from a TEX/LATEX file prepared by the author.